Opto-Electronic Advances

Supplementary information

August 2023, Vol. 6, No. 8

DOI: 10.29026/oea.2023.220174

Third-harmonic generation and imaging with resonant Si membrane metasurface

Ze Zheng[1], Lei Xu[1*], Lujun Huang[2,3], Daria Smirnova[4], Khosro Zangeneh Kamali[4], Arman Yousefi[1], Fu Deng[5], Rocio Camacho-Morales[4], Cuifeng Ying[1], Andrey E. Miroshnichenko[2], Dragomir N. Neshev[4] and Mohsen Rahmani[1*]

[1]Advanced Optics and Photonics Laboratory, Department of Engineering, School of Science & Technology, Nottingham Trent University, Nottingham NG11 8NS, UK; [2]School of Engineering and Information Technology, University of New South Wales, Canberra ACT 2600, Australia; [3]School of Physics and Electronic Science, East China Normal University, Shanghai 200241, China; [4]ARC Centre of Excellence for Transformative Meta-Optical Systems (TMOS), Research School of Physics, The Australian National University, Canberra ACT 2601, Australia; [5]Department of Physics, Hong Kong University of Science and Technology, Kowloon, Hong Kong SAR, China.

*Correspondence: L Xu, E-mail: lei.xu@ntu.ac.uk; M Rahmani, E-mail: mohsen.rahmani@ntu.ac.uk

This file includes:

Supplementary information for this paper is available at https://doi.org/10.29026/oea.2023.220174

Section 1: Band structure and mode profile for silicon disk metasurface

Figure S1 shows the calculated band structure for the silicon disk metasurface with the same unit cell (inverse-designed counterpart to the dimer-hole metasurface shown in Fig. 1 of the main text). As can be seen, the mode of the same nature is located at a spectral position of 882 nm. To shift the mode to 1510 nm (as the mode for the membrane metasurface), it requires a much larger size for both the unit cell and the silicon disks. Furthermore, the electric field of light is mainly located near the silicon/air interface and outside the silicon disk. This clearly shows that by utlising the membrane metasurfaces, under the same unit size, we can achieve strong field enhancement at a higher spectral position compared to disk metasurfaces (from 882 nm to 1510 nm).

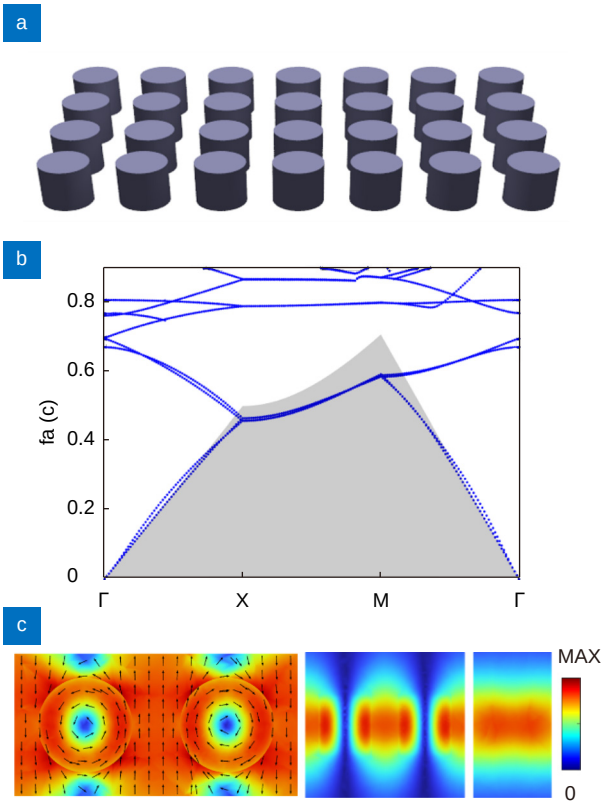

Fig. S1 | (**a**) Schematic representation of the designed silicon membrane metasurface. (**b**) Calculated bandgap structure for the metasurface. (**c**) Near-field electric distributions for the mode TE(3, 1, 1).

Section 2: Multipolar structure and field distribution for the Fano resonance near 1000 nm

As shown in Fig. S3(b), the resonance shows a clear Fano shape spectrum based on the simulation. The resonance is dominated by the interference between the electric dipole, quadrupole, and magnetic octupole (see Fig. S3(a)). Via tuning the offset $\mathbf{x}_0$, the mode TE(3,2,1) is transformed into the resonance, which can be seen by contrasting the electric distributions between Fig. 2(b) and Fig. S3(c).

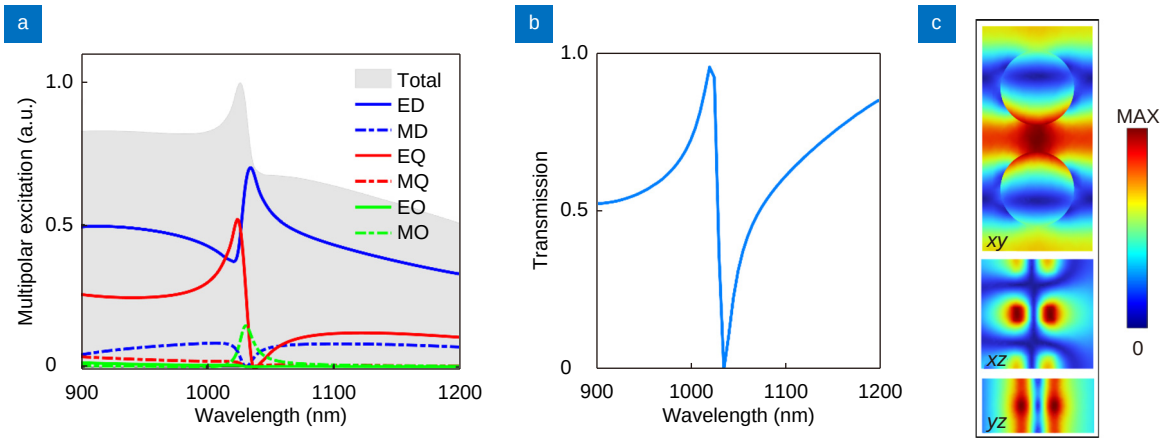

Fig. S2 | Calculated linear spherical multipolar structure (a) transmission spectra (b) and the electric near-field distribution (c) for the Fano resonance around 1000 nm.

Section 3: Comparison of unit sizes and conversion efficiencies for silicon metasurfaces

Table S1 summarises the input powers, spectral wavelength of resonance, unit cell sizes, Q-factors, and conversion efficiencies for silicon metasurfaces. For making a fair comparison, we utilise two approaches to calculate the conversion efficiencies of those works: 1) $\eta_{\mathrm{THG}} = P_{\mathrm{THG}}/P_{\mathrm{input}}$; 2) $\eta'_{\mathrm{THG}} = P_{\mathrm{THG}}/(P_{\mathrm{d}}^3 \tau f_{\mathrm{rep}} S_{\mathrm{beam}})$, where $P_{\mathrm{d}} = P_{\mathrm{input}}/(\tau f_{\mathrm{rep}} S_{\mathrm{beam}})$. In the second approach, the efficiency is no longer dependent on the level of input power or the size of beam spot, which is more corresponding to the nonlinear performance of silicon metasurfaces compared to the first way. In addition, the first approach directly exhibits the process of energy conversion from linear range to nonlinear range. Due to the reasons revealed above, we keep both methods for comparison.

By designing the Q-factor to match the resonance width with the laser pulse, membrane metasurfaces enable a strong coupling of incident light into the resonance and nonlinear light-matter interactions. Among those working in the NIR spectral region, membrane metasurfaces have obtained a comparable conversion efficiency with a unit-cell size, less than half of other metasurfaces.

Table S1 | Comparison of unit cell sizes, Q-factors and conversion efficiencies measured for silicon metasurfaces.

	Ref.[52] (2014)	Ref.[53] (2015)	Ref.[34] (2019)	Ref.[50] (2019)	Our work
Input power (P_{input})	30 mW	50 mW	100 mW	3.2 mW	21.2 mW
Wavelength	1240 nm	1348 nm	1345 nm	1588 nm	~1500 nm
Unit cell size	500×500 nm	750×750 nm	840×840 nm	720×720 nm	300×600 nm
Q-factor	~12	466	~112	18511	~75
Conversion efficiency ($\eta_{\mathrm{THG}} = P_{\mathrm{THG}}/P_{\mathrm{input}}$)	1.3×10^{-7}	1.2×10^{-6}	5×10^{-6}	9.1×10^{-7}	3.6×10^{-6}
Conversion efficiency ($\eta'_{\mathrm{THG}} = P_{\mathrm{THG}}/P^3_{\mathrm{d}}S_{\mathrm{beam}}$)	-	9.72×10^{-21} W^{-2}·cm^4	2.05×10^{-20} W^{-2}·cm^4	1.15×10^{-18} W^{-2}·cm^4	2.23×10^{-19} W^{-2}·cm^4

Table S2 | The experimental parameters used to calculate silicon metasurfaces' conversion efficiencies, including input powers, laser pulse durations, repetition rates, beam spot sizes, and THG emissions.

	Ref.[52] (2014)	Ref.[53] (2015)	Ref.[34] (2019)	Ref.[50] (2019)	Our work
Input power (P_{input})	30 mW	50 mW	100 mW	3.2 mW	21.2 mW
Laser pulse duration (τ)	-	250 fs	200 fs	5 ps	150 fs
Repetition rate (f_{rep})	-	80 MHz	80 MHz	80 MHz	80 MHz
Beam spot size (S_{beam})	-	~225 μm^2	~400 μm^2	~9 μm^2	~441 μm^2
THG emission (P_{THG})	-	~60 nW	~500 nW	2.92 nW	76 nW